How to Speed up Ion Transport in Nanopores

Konrad Breitsprecher,[1] Mathijs Janssen,[2,3] Pattarachai Srimuk,[4,5] B. Layla Mehdi,[6] Volker Presser,[4,5] Christian Holm,[1] and Svyatoslav Kondrat[7]

[1]*Institute for Computational Physics, Universität Stuttgart, Allmandring 3, 70569 Stuttgart, Germany*

[2]*Max-Planck-Institut für Intelligente Systeme, Heisenbergstraße 3, 70569 Stuttgart, Germany*

[3]*IV. Institut für Theoretische Physik, Universität Stuttgart, Pfaffenwaldring 57, 70569 Stuttgart, Germany**

[4]*INM - Leibniz Institute for New Materials, Campus D2 2, 66123 Saarbrücken, Germany*

[5]*Department of Materials Science and Engineering, Saarland University, Campus D2 2, 66123, Saarbrücken, Germany*

[6]*University of Liverpool, School of Engineering, 514 Brodie Hall, L69 3GQ, Liverpool, United Kingdom*

[7]*Department of Complex Systems, Institute of Physical Chemistry, PAS, Kasprzaka 44/52, 01-224 Warsaw, Poland*

Subnanometre pores exhibit exciting physics and play an increasingly important role in science and technology. However, while electrolyte-filled ultranarrow pores provide excellent capacitive characteristics, as in supercapacitors, ions experience difficulties in entering and leaving such pores, which slows down charging and discharging processes. In an earlier work we showed for a simple model that a slow voltage sweep charges ultranarrow pores quicker than an abrupt voltage step. A slowly applied voltage avoids ionic clogging and co-ion trapping—a problem known to occur when the applied potential is varied too quickly—causing sluggish dynamics. Herein, we verify this finding experimentally. Guided by theoretical considerations, we develop a *non-linear* voltage sweep and demonstrate, with molecular dynamics simulations, that it can charge a nanopore even faster than the corresponding optimized linear sweep. For discharging we find, with simulations and in experiments, that if we reverse the applied potential and then sweep it to zero, the pores lose their

charge much quicker than they do for a short-circuited discharge over their internal resistance. Our findings open up opportunities to greatly accelerate charging and discharging of subnanometre pores without compromising the capacitive characteristics, improving their importance for energy storage, capacitive deionization, and electrochemical heat harvesting.

Keywords: porous carbons, subnanometre pores, ionic liquids, charging dynamics, discharging, optimization, nonlinear potential difference sweeps, molecular dynamics simulations, experiments

Electrolyte-immersed porous electrodes are an essential building block for many state-of-the-art technologies in energy storage [1–4], energy harvesting [5–7] and capacitive deionization [8–10]. Of particular importance are electrical double-layer capacitors (EDLCs), often called supercapacitors or ultracapacitors [1–4, 6, 11, 12], that store energy by electrosorption of ionic charge into the porous electrodes. Their performance is characterized by the energy density $\mathcal{E}$ and power density $\mathcal{P}$, which describe the amount of energy and the speed with which it can be supplied to an external load or device. Owing to their particular $(\mathcal{E}, \mathcal{P})$ properties, supercapacitors find their way in applications that need higher power than delivered by batteries and more energy than stored in traditional dielectric capacitors. So far the highest achievable capacitance [13–15] and energy densities [16] have been obtained with nanometre-sized pores. Whence an extensive research effort has been dedicated to understanding the properties of such *nanoporous* supercapacitors [12, 17–28], with an overarching goal being to maximize the stored energy density [29–36] and the speed of charging and discharging [37–42].

It is often assumed that charging and discharging times are equal and proportional to the time constant $\mathcal{E}/\mathcal{P}$ [2]. This reasoning probably originates from simple electronic RC circuits, which indeed display a charge/discharge symmetry (Supplementary Note S1). However, even for a simple EDLC model with planar electrodes, such charge/discharge symmetry is only present at small applied potentials [43–45]. Molecular dynamics simulations have demonstrated that also nanopores charge and discharge in a dissimilar fashion [42]. The knowledge of discharging behaviour is thus insufficient for predicting charging behaviour and *vice versa*. Therefore, in this article, which centres around charge-discharge time opti-

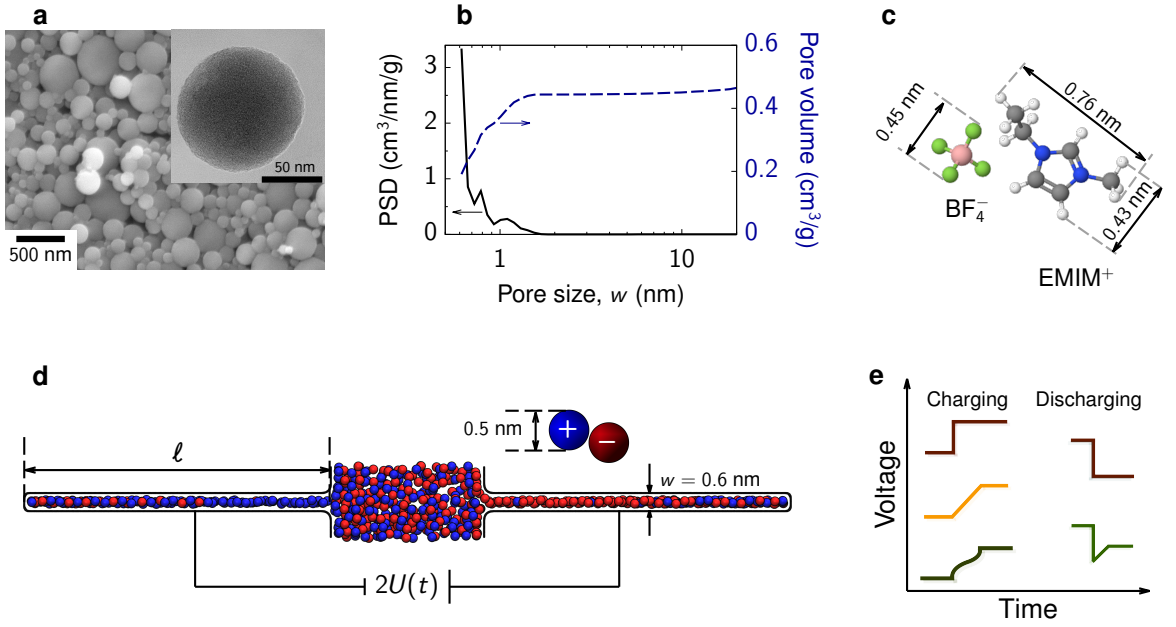

FIG. 1. **Systems and charge-discharge voltage sweeps.** **a**, SEM and BF-STEM (the inset) images of novolac-derived porous carbon particles. **b**, Pore-size distribution (PSD) and cumulative PSD of the novolac-derived porous electrodes. **c**, Schematic drawings and sizes of EMIM-BF_4 ionic liquid used in the experiments. **d**, Simulation model of a supercapacitor and an ionic liquid. Ions were modeled as charged spheres, and each electrode consisted of one slit nanopore. The accessible pore width $w = 0.6\,\text{nm}$ and the ion diameter $a = 0.5\,\text{nm}$ have been used in all simulations. The pore length ℓ was 12 nm, 16 nm, and 20 nm. **e**, Schematics of cell voltages used in this study for charging and discharging supercapacitors.

mization, we consider charging and discharging separately. Furthermore, as charge and discharge times are complicated functions of many parameters, any optimization study should specify which parameters are varied and which are kept fixed. One could ask, for instance, given a charging or discharging procedure (voltage step or sweep, *etc.*), which supercapacitor charges/discharges the fastest? This is a geometric problem of minimizing internal resistances via different pore shapes, lengths, *etc.* [42, 46]. An alternative question that one could ask is: *Given a supercapacitor*, which time-dependent cell voltage minimizes the time spent to charge it to a certain charge Q, or to discharge the same supercapacitor to $Q = 0$? In this article, we focus on the second question. Finding the voltage sweeps providing the shortest charging times is of practical importance to supercapacitors. Finding

optimal *discharging* sweeps, which we also set out to do, is relevant to electrochemical low-grade heat harvesting [7] and capacitive deionization [8–10], where operation speed may be more important than energy efficiency.

Recent molecular dynamics (MD) simulations have shown that, when a potential difference is applied abruptly to a nanopore, counter-ions rush to the pore's entrance and clog the pore, causing co-ion trapping deep in its interior and leading to an overall sluggish charging dynamics [42, 47, 48]. Pore clogging can be avoided by applying the potential difference with a linear sweep, that is, by varying it with a constant rate [42] (Fig. 1e). We show in this article that charging can be made even faster than the fastest (optimized) linear sweep, if the variation of the applied potential is matched to the actual rate of co-ion desorption. We propose a general expression for a non-linear sweep function and consider two closed-form approximations. We assess the benefits of such a non-linear voltage sweep in MD simulations of a model supercapacitor and in experiments with novolac-derived carbon electrodes (Fig. 1). Finally, our MD simulations and experiments show that a nanopore *discharges* faster if, instead of a step to zero volt, we apply a non-linear sweep consisting of a voltage inversion followed by a linear sweep to zero.

NON-LINEAR VOLTAGE SWEEP TO ACCELERATE CHARGING

As has been shown by simulations [42, 47, 48], charging ultra-narrow pores with a large voltage step leads to counter-ions crowding the pore entrances, which induces trapping of co-ions inside the pores. To charge a pore faster, co-ions must be given enough time to diffuse out of the pore before the onset of any possible crowding. For a tiny increment ΔV of the applied potential—much too small to yield pore clogging—the co-ion desorption time can be estimated as $\Delta t = l^2/D_\mathrm{c}$, where D_c is the in-pore co-ion diffusion constant and l the distance of the co-ion to the pore exit. Then the rate of an optimal *linear* sweep can be approximated by $k_\mathrm{opt} = \Delta V/\Delta t_\mathrm{max}$, with Δt_max being the longest of these times [42]. However, as Δt may differ from Δt_max at different stages of charging, it may be possible to charge a nanopore faster than with the optimized linear sweep, by varying Δt, and hence the sweeping rate k, in the course of charging.

Derivation of the non-linear sweep function

Before the potential difference U is applied to a nanopore, the distribution of co-ions in a pore is homogeneous. These co-ions can be split into K_0 ($\approx \rho_c^0 w\ell a$) imaginary 'layers' along the pore, where ρ_c^0 is the in-pore co-ion density at $U = 0\,\mathrm{V}$, w is the slit width and ℓ is its length, and a is the ion diameter, for simplicity assumed the same for cations and anions. One can then apply the potential difference in steps, allowing exactly one layer of co-ions to diffuse out during each step. Assuming that the co-ions redistribute homogeneously in each step, the diffusion path during the n^{th} step is $l = \ell/(K_0 - n - 1)$, so that the distance between the layers increases with increasing n (note, however, that the system does not have to equilibrate in each step). The time needed by a co-ion layer to leave the pore during n^{th} step is then

$$\Delta t_n = \frac{1}{D_c(n)} \frac{\ell^2}{(K_0 - n + 1)^2}, \tag{1}$$

where the co-ion diffusion coefficient D_c may depend on the current state of the system (*i.e.*, on n). The total time t needed to charge a nanopore to potential difference U is the sum of all time increments up to $n = K_0 - K(U)$, where $K(U)$ is the number of layers in the pore at U, that is, $t(U) = \sum_{n=0}^{K_0 - K(U)} \Delta t_n$. Approximating this sum by an integral over n, and changing the integration variable from n to voltage u, we find

$$t(U) \approx -\ell^2 \int_0^U \frac{(dK/du)}{D_c(u)[K(u)+1]^2} du. \tag{2}$$

Equation (2) is an implicit equation for the time-dependent sweep function $U(t)$ in terms of $K(U)$. To demonstrate its applicability, we have numerically determined $K(U)$ for the model supercapacitor shown in Fig. 1 with MD simulations; the results are shown by symbols in Fig. 2a. Assuming that D_c does not depend on the applied potential, we performed the integration in eq. (2) numerically using the composite trapezoidal rule (symbols in Fig. 2b; see also Figs. S3 and S4). The results demonstrate that $U(t)$ can be varied quickly at early times, corresponding to low voltages, which is because there is still a sufficient amount of co-ions close to the pore exit, and hence their 'effusion' path is relatively short (*i.e.*, the path over which the co-ions need to diffuse to exit the pore). At intermediate times, corresponding to intermediate voltages, this effusion path becomes longer due to the reduced co-ion density and one must slow down the variation of the applied potential, to allow the co-ions to leave

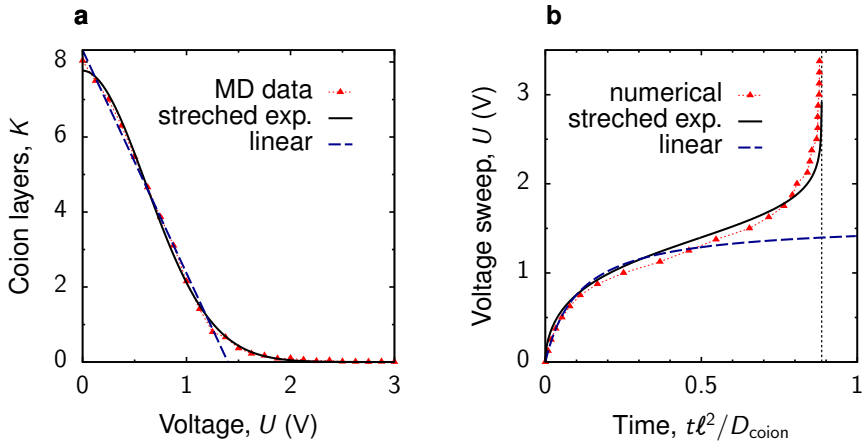

FIG. 2. **Determination of non-linear sweep function.** **a**, Number of co-ion layers in a nanopore, K, as a function of potential U applied to the pore with respect to the bulk electrolyte. Symbols denote the values obtained from MD simulations of a model supercapacitor (Fig. 1d). K was calculated as $K = \rho_c w\ell a = N_c a/h$, where $\rho_c = N_c/(w\ell h)$ and N_c are the density and the number of co-ions in a pore, respectively, a is the ion diameter, and w, ℓ and h are the width, length and height of the pore; K_0 is the value of K at $U = 0\,\mathrm{V}$. The solid and dashed lines are approximations to these data by stretched exponential (eq. (3)) and linear (eq. (7)) functions, respectively. Pore width $w = 0.6\,\mathrm{nm}$ and length $\ell = 12\,\mathrm{nm}$; for other pore lengths see Figs. S3 and S4, and for the fitting parameters see Fig. S5. **b**, Non-linear voltage sweeps as obtained by numerically integrating eq. (2) with the MD data for $K(U)$ from panel (a), and by using the stretch exponential and linear approximations for $K(U)$; the corresponding non-linear sweep functions are given by eqs. (6) and (9), respectively. The thin dotted line shows $t = \tau$, where $U(t)$ diverges, see eqs. (5) and (6).

the pore. Finally, at long times (higher applied potentials), there are practically no co-ions left in the pore and the charging can proceed in an almost step-wise manner.

Stretched exponential approximation

To complement the above insights from the numerical evaluation of eq. (2), we approximated the simulation data of $K(U)$ by a stretched exponential

$$K(U) = K_0 \exp\left[-(\gamma U)^{\alpha}\right], \tag{3}$$

where K_0, γ, and α are ℓ-dependent fitting parameters, allowing us to perform the integral in eq. (2) analytically. We have used the dogleg least square algorithm from `scipy` (`https://scipy.org`), to fit eq. (3) to the MD data. Figure 2a demonstrates that eq. (3) fits the MD data decently (solid line in Fig. 2a, see also Figs. S3, S4, and S5). Notably, we found that the fitting parameters α and γ depend weakly on the pore length, ℓ, while K_0 varies with ℓ more significantly (*viz.*, $K_0 \sim \ell$, see Fig. S5). This is understandable as α and γ define the shape of $K(U)$, which does not change appreciably with ℓ (Fig. S5), while K_0 represents the number of co-ion layers in the pore at $U = 0$ V, which should indeed increase with the pore length.

Plugging eq. (3) into eq. (2) and assuming again that D_c is U-independent, one finds

$$t(U) = \tau \frac{1 - K(U)/K_0}{1 + K(U)}, \tag{4}$$

where

$$\tau = \frac{\ell^2}{D_\mathrm{c}} \frac{K_0}{K_0 + 1}. \tag{5}$$

Inverting eq. (4) leads to

$$U(t) = \gamma^{-1} \left(\ln \frac{1 + K_0 t/\tau}{1 - t/\tau} \right)^{1/\alpha}. \tag{6}$$

Figure 2b shows that eq. (6) provides a good approximation to the non-linear sweep function obtained by integrating eq. (2) numerically. For very long pores, $\ell \gg (\rho_\mathrm{c}^0 w a)^{-1}$, one has $K_0 \gg 1$ and eq. (5) gives $\tau \sim \ell^2$ in the leading order in ℓ. Then eq. (4) leads to charging times $t(U) \sim \ell$ at potential differences below threshold $U_t = \gamma^{-1} (\ln K_0)^{1/\alpha}$, and $t(U) \sim \ell^2$ at $U \gg U_t$ (at which $K(U) \approx 0$). The latter result is in line with the quadratic pore-length scaling of the charging times of optimal linear sweep [42].

Linear approximation

While the stretched exponential (eq. (3)) approximates the number of co-ion layers $K(U)$ for all applied potentials considered (Fig. 2a), the resulting expression for the non-linear sweep function, eq. (6), looks cumbersome. A useful approximation can be obtained for low voltages, $U \lesssim 1.3\,\mathrm{V}$ in Fig. 2a, likely most relevant to experimental systems [25, 27, 49]. This can be done by noticing that $K(U)$ varies roughly linearly in this regime, *i.e.*

$$K(U) = K_0(1 - \gamma U), \tag{7}$$

where γ and K_0 are again ℓ-dependent fitting parameters. We have fitted the MD data for $U \lesssim 1.3\,\mathrm{V}$ to eq. (7) (dash line in Fig. 2a, Fig. S6) using the dogleg least square algorithm from `scipy` (`https://scipy.org`).

Plugging eq. (7) into eq. (2) and assuming D_c to be U independent, as before, one obtains

$$t(U) = \frac{\tau\,\gamma U}{1 + K(U)}, \tag{8}$$

where τ is given by eq. (5). Inverting eq. (8) yields a simple equation

$$U(t) = \frac{U_0\,t}{t + \tilde{\tau}} \tag{9}$$

where $U_0 = (1 + K_0)/(\gamma K_0)$ and $\tilde{\tau} = \tau/K_0$, with τ given by eq. (5). It is interesting to note that the linear approximation for $K(U)$, eq. (7), still yields a sweep function, eq. (9), that varies non-linearly with time.

Figure 2b shows that eq. (9) approximates the non-linear sweep function (obtained by numerical integration of eq. (2)) at low voltages well, but fails at high voltages. This is not surprising, as we fitted the linear approximation only in the low-voltage regime.

For long pores, $\ell \gg 1/(\rho_\mathrm{c} w a)$, one has $\tau \sim \ell^2$, and eq. (8) gives $t(U) \approx [\ell^2/(D_\mathrm{c} K_0)][\gamma U/(1-\gamma U)]$. Since $K_0 \sim \ell$ and γ depend only weakly on ℓ (Fig. S6), the charging time increases proportionally to the pore length, ℓ. This linear ℓ-scaling is in line with the scaling found for the stretched exponential approximation at low applied potentials, and unlike the optimal linear sweep, for which the charging times scale quadratically with ℓ [42].

Results of MD simulations

To assess the benefits of the nonlinear sweeps, as compared to step-voltage and optimal linear sweeps [42], we performed MD simulations, in which we applied these three different charging protocols to the model supercapacitor shown in Fig. 1d. For the non-linear sweep function, we used eq. (6), as obtained by fitting the stretched exponential approximation to the MD data for $K(U)$ (Fig. 2). Equation (6) depends parametrically on τ, which, in turn, depends on the unknown co-ion diffusion coefficient D_c (eq. (5)). Accordingly, we treated τ as an optimization parameter and performed MD simulations with the non-linear sweep functions for several values of τ. Examples of $U(t)$ for $\tau = 4\,\mathrm{ns}$ and $\tau = 12\,\mathrm{ns}$ are shown in Fig. 3a. Figure 3a also shows the accumulated charge and the number of counter and

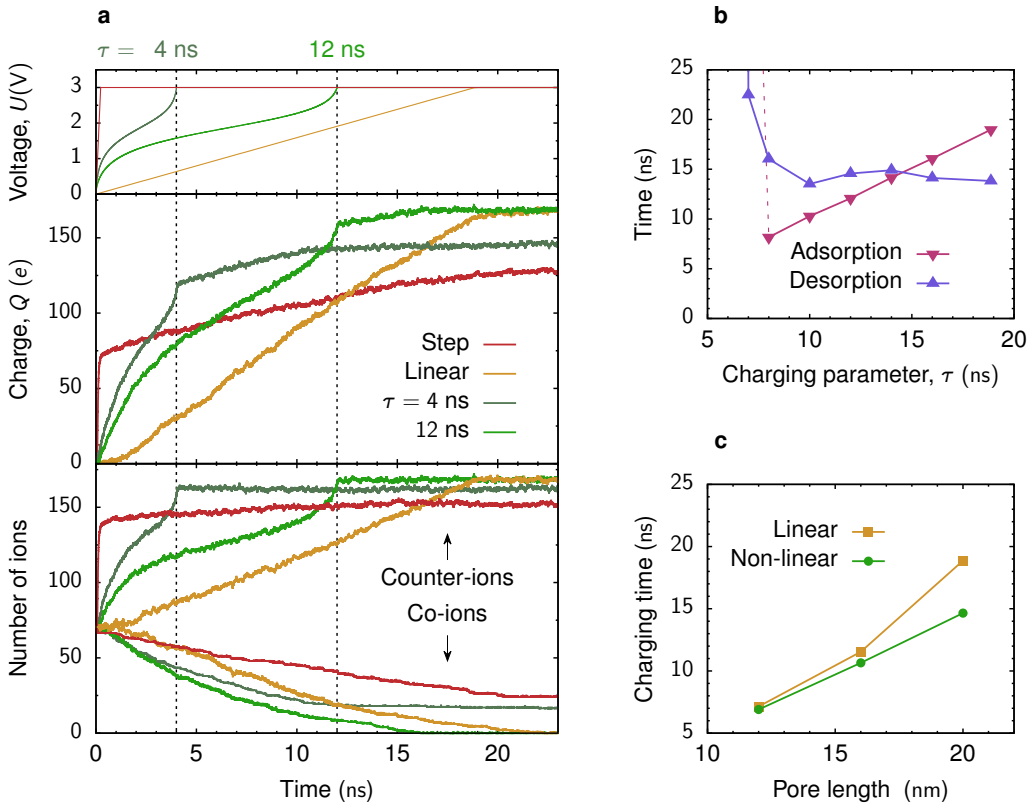

FIG. 3. **Non-linear sweeps versus step-voltage and optimal linear sweep.** **a**, Potential $U(t)$ applied to a nanopore with respect to the bulk electrolyte (top), accumulated charge (middle) and the number of ions (bottom) for step-voltage, linear and non-linear sweep charging from MD simulations. $U(t)$ has been obtained via fitting the MD data to the stretched exponential (see eq. (3) and Fig. 2), and τ is an 'optimization' parameter, see eqs. (5) and (6). **b**, Adsorption and desorption times as functions of parameter τ. The optimal τ value, $\tau_{\rm opt}$, corresponds to τ at which the adsorption and desorption times intersect. **c**, Charging times for linear and non-linear sweeps as functions of pore length. In all plots the pore width is $w = 0.6\,$nm and the length $\ell = 20\,$nm.

co-ions inside the pore as a function of time. Clearly, the non-linear sweep provides faster charging than the step-voltage for all τ considered. Compared to the optimal linear sweep, the non-linear sweep charges faster only for some τ values. When sweeps are too fast (small τ), co-ion trapping leads to sluggish desorption, as is the case for the step-voltage charging or too-fast linear sweeps (red and dark-green curves in Fig. 3a). For sufficiently large τ, the co-ion desorption proceeds faster than for the optimal linear sweep, as anticipated (orange

vs light-green curves in Fig. 3a).

Figure 3b shows the τ-dependence of the co-ion desorption and counter-ion adsorption times. This figure demonstrates that the desorption time increases drastically for small τ, which is due to co-ion trapping, and levels off for larger values of τ. The adsorption time increases roughly linearly with τ for $\tau > 8\,\mathrm{ns}$, but increases abruptly for smaller values of τ (see also Fig. 3a). Figure 3b shows that the *optimal* τ value, τ_{opt}, that is, the value that minimizes the charging time, can be found as a crossing point of adsorption and desorption times (there might be more than one crossing; clearly, τ_{opt} corresponds to the one providing the shortest time).

Next, we performed MD simulations for a few pore lengths ℓ and determined τ_{opt} in each case. From the accumulated charge Q (obtained at τ_{opt}), we extracted the charging time, t_{charge}, which we defined as the time at which Q reaches 96% of the maximum charge capacity at a given applied potential (note that the so determined t_{charge} is only approximately equal to $t(U)$, eq. (4), since we allowed for 4% tolerance in co-ion desorption, to be consistent with ref. [42]). The results are shown in Fig. 3c, along with the charging times obtained by the optimal linear sweep [42]. The difference between the charging times for the linear and non-linear sweep functions increases markedly with the pore length, ℓ. The data suggest a linear increase of t_{charge} with ℓ in the latter case, consistent with the asymptotic analysis below eq. (6). In the former case $t_{\mathrm{charge}} \sim \ell^2$ [42]. This indicates that the nonlinear sweeps may provide significantly faster charging for longer pores.

Experimental results

To test our theoretical findings, we have performed charging experiments with a supercapacitor based on a symmetric two-electrode setup and novolac-derived, activated carbon with well-controlled nanopores as the electrode material [50] (Fig. 1a,b). As seen from the gas sorption data, the pore size distribution is very narrow with an average pore size of 0.68 nm and a total pore volume of $0.49\,\mathrm{cm}^3/\mathrm{g}$. We used EMIM-$BF_4$ room-temperature ionic liquid as electrolyte (Fig. 1c).

We first applied a step-like cell voltage to the supercapacitor and measured how the accumulated charge varies over time (the solid red lines in Fig. 4). We found that the charge can be fitted decently by the sum of two exponents [39], $Q(t) = Q_\infty[1 - a_1 \exp(-t/\tau_1) -$

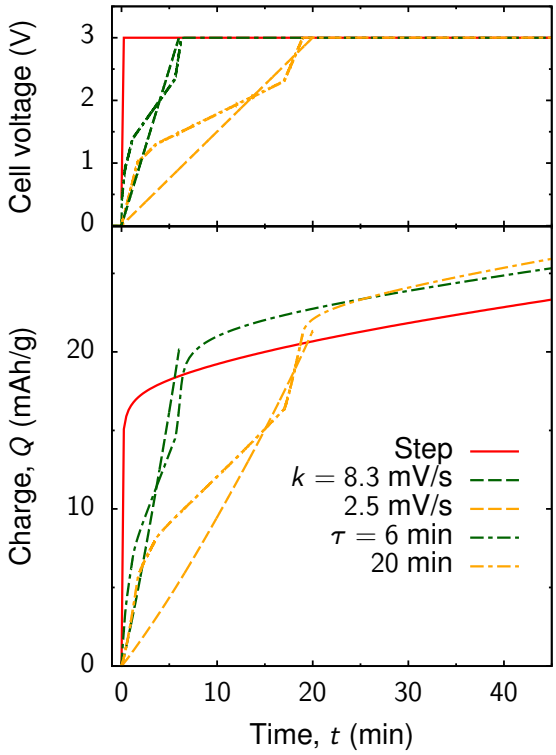

FIG. 4. **Non-linear sweeps versus step-voltage and linear sweeps for novolac-derived carbons.** Cell voltage (top) and accumulated charge (bottom) for step-voltage, linear and non-linear sweep charging. For the non-linear sweeps, cell voltage *vs* time have been obtained by using the stretched exponential approximation (see eq. (3)), for two values of τ, as indicated on the plot. The linear sweeps have been obtained via a one-cycle voltammetry; the discharging parts of these curves are not shown for clarity.

$a_2 \exp(-t/\tau_2)]$ (for the fitting parameters and the plot see Fig. S7). The slow timescale $\tau_2 \approx 45\,\text{min}$ is in agreement with model predictions saying that supercapacitors charge at late times with the timescale $\tau = \alpha(L/2 + H)^2/D \approx 17\,\text{min}$ [51], where $L \approx 150\,\mu\text{m}$ is the electrode separation (the thickness of a separator), $H \approx 109\,\mu\text{m}$ the electrode thickness, $D \approx 10^{-11}\,\text{m}^2/\text{s}$ the bulk diffusion constant of EMIM-BF_4, and α is a salt-concentration dependent factor (of order unity for dilute electrolytes) [51]. As our supercapacitor model contains just two pores and a nanometer-sized reservoir (Fig. 1d), and hence does not account for the multiscale nature of real supercapacitors, this slow diffusive response is absent in our MD simulations.

We next studied how this abrupt step-voltage charging compares with slower voltage sweeps. We generated non-linear sweep data in a computer for a few values of τ according to eq. (6), similarly as in the simulations. The non-linear sweeps were produced by a piecewise approximation via linear functions (dash-dot lines in the top plot of Fig. 4). To study the linear sweep charging, we used a 'single-cycle' voltammetry; the single run, rather than cycling, was necessary to ensure that initially the supercapacitor was fully discharged. The sweep rates k were chosen such that the times $\tau_k = U/k$ ($U = 3\,\mathrm{V}$ is the applied cell voltage) were comparable to the values of τ used in the non-linear sweeps. (In the voltammetric experiments the cell voltage was swept to zero and the device was allowed to discharge after reaching the final value of 3 V. For simplicity, we show only the charging parts of these $Q(t)$ curves in Fig. 4.)

Figure 4 shows that the voltage step is overtaken by all four slower applied potentials. This constitutes the first experimental verification of ref. [42], which suggested that a step-voltage does worse than linear sweep charging. We note, however, that both the linear and non-linear sweeps have not been optimized and hence, unlike in the simulations (Fig. 3), the charge in Fig. 4 continues to grow after the cell voltage reaches its final value.

While our experiments have demonstrated that a slow variation of applied potential can make charging faster than the step-voltage, they were inconclusive regarding the comparison of the linear and non-linear sweeps (we note, however, that the nonlinear sweep with $\tau = 20\,\mathrm{min}$ performed slightly better than the corresponding linear sweep with $k = 2.5\,\mathrm{mV/s}$, which is consistent with the simulations). This is likely because we have not reached the optimal sweep rate, which appeared to be slower than 0.1 mV/s (Fig. S8), implying that the time needed to fully charge the supercapacitor was greater than 8 h. Thus, the voltage sweeps in the experiments operated only in short times (compare with $\tau = 4\,\mathrm{ns}$ in Fig. 3a). Nevertheless, both the simulations and the experiments clearly demonstrate that 'slow' voltage sweeps have the potential to speed up charging.

ACCELERATING DISCHARGING BY VOLTAGE INVERSION

Turning to the discharging of supercapacitors, we are interested in the quickest discharging voltage sweep $U(t)$ that takes a supercapacitor from a charged state at applied potential $U_{\mathrm{ch}} > 0\,\mathrm{V}$ to the fully discharged state, which corresponds to $U = 0\,\mathrm{V}$. It has been sug-

gested [42] that the *optimal linear* discharging sweep is as fast as possible, that is, via a step to $U = 0\,\mathrm{V}$. This is different from optimal *charging* with a gentle voltage sweep because, for discharging, there is no danger of clogging the pore entrance either with co-ions or counter-ions. But could discharging be even faster than what is achieved by a step voltage? This may be expected for an electrical double-layer capacitor with *planar* electrodes, which has been successfully modeled for low voltages through an equivalent RC circuit [52] (see also [46]). The dielectric capacitor of such a circuit can be discharged 'instantaneously' by applying a negative delta-like spike (as obtained from the mathematical model, ignoring dissipation, see Supplementary Note S1), suggesting that an analogous sped-up discharging could be achieved for the corresponding double layer capacitor (note, however, that the applicability of the circuit model to double-layer capacitors might be questionable for such a spike). For a *nanoporous* supercapacitor, it is unclear how a negative applied potential could speed up counter-ion desorption, as the electric field vanishes inside nanopores [53]. But there might well be pore-entrance effects. For instance, applying a negative potential difference to a nanopore may deplete counter-ions from the pore entrance area, leaving the counter-ion desorption akin to an expansion of a gas into a vacuum, which is faster than into a finite density gas. However, applying a too-negative potential difference may clog the pore entrance with co-ions, in the same way as the attracted counter-ions impede co-ion desorption in the charging process. To discern these two competing phenomena, we have studied the behaviour of our supercapacitors upon discharging via a *voltage-inversion* discharging sweep (Fig. 1)

$$U(t) = \begin{cases} U_{\mathrm{ch}} > 0 & \text{if } t \leq 0, \\ U_{\mathrm{inv}} + k_{\mathrm{inv}} t & \text{if } 0 < t < \tau_{\mathrm{inv}}, \\ 0 & \text{if } t \geq \tau_{\mathrm{inv}}, \end{cases} \tag{10}$$

where k_{inv} is the slope with which the voltage approaches $U = 0\,\mathrm{V}$ after a voltage inversion of magnitude $U_{\mathrm{inv}} < 0\,\mathrm{V}$ at time $t = 0$, and $\tau_{\mathrm{inv}} = -U_{\mathrm{inv}}/k_{\mathrm{inv}}$ is the time at which $U = 0\,\mathrm{V}$.

Results of MD simulations

Figure 5 shows examples of $U(t)$ given by eq. (10) for a few values of U_{inv} and k_{inv}, along with the corresponding numbers of co and counter ions obtained by MD simulations. To analyse this discharging behaviour, we first consider how discharging profiles vary with k_{inv}.

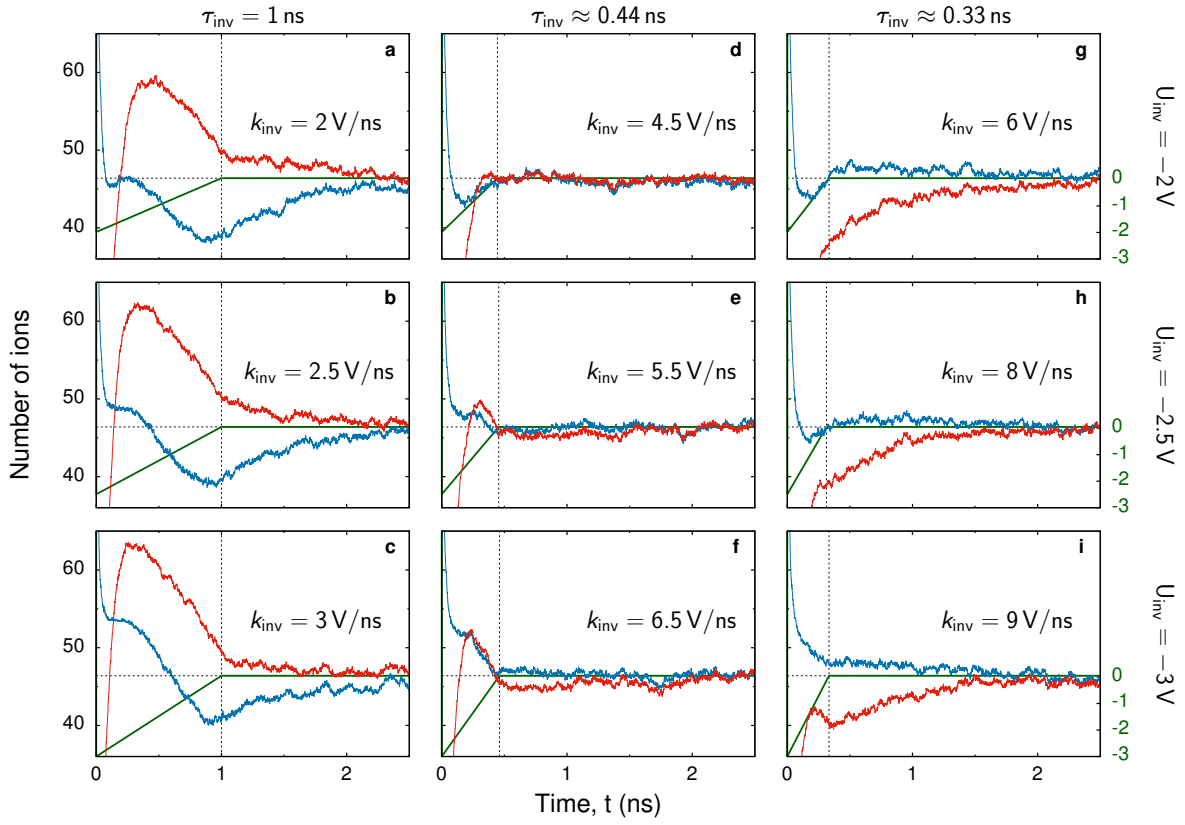

FIG. 5. **Discharging via voltage inversion.** Discharging profiles are shown for a few values of the inversion voltage $U_{\rm inv}$ (measured with respect to the bulk electrolyte) and slope $k_{\rm inv}$ with which the voltage reverses to approach $U = 0$, see eq. (10). The rows correspond to the same values of $U_{\rm inv}$, as indicated in the plot, and the columns to (approximately) the same values of $\tau_{\rm inv} = -U_{\rm inv}/k_{\rm inv}$ (thin vertical lines). The voltage and the numbers of co and counter-ions in the pore are shown by green, red, and blue lines, respectively. Thin horizontal lines denote the equilibrium numbers of co and counter-ions at $U = 0$. The optimal discharging parameters, minimizing the discharging time, are $U_{\rm inv} = -2.5\,{\rm V}$ and $\tau_{\rm inv} \approx 0.4$ ($k_{\rm inv} = 5.5\,{\rm V/ns}$, *cf.*, Fig. 6). In all plots the pore width is $w = 0.6\,{\rm nm}$ and the length $\ell = 12\,{\rm nm}$.

When $k_{\rm inv}$ is too small, that is, when the applied potential reverses to zero too slowly, the co and counter ions greatly overshoot their final values. This process is then followed by a slow relaxation to equilibrium, evidently giving long discharging times (Fig. 5a-c). When $k_{\rm inv}$ is too high, that is, when the application time of the (varying) negative potential difference is too short (small $\tau_{\rm inv} = -U_{\rm inv}/k_{\rm inv}$), then co and counter-ions 'undershoot' and discharging

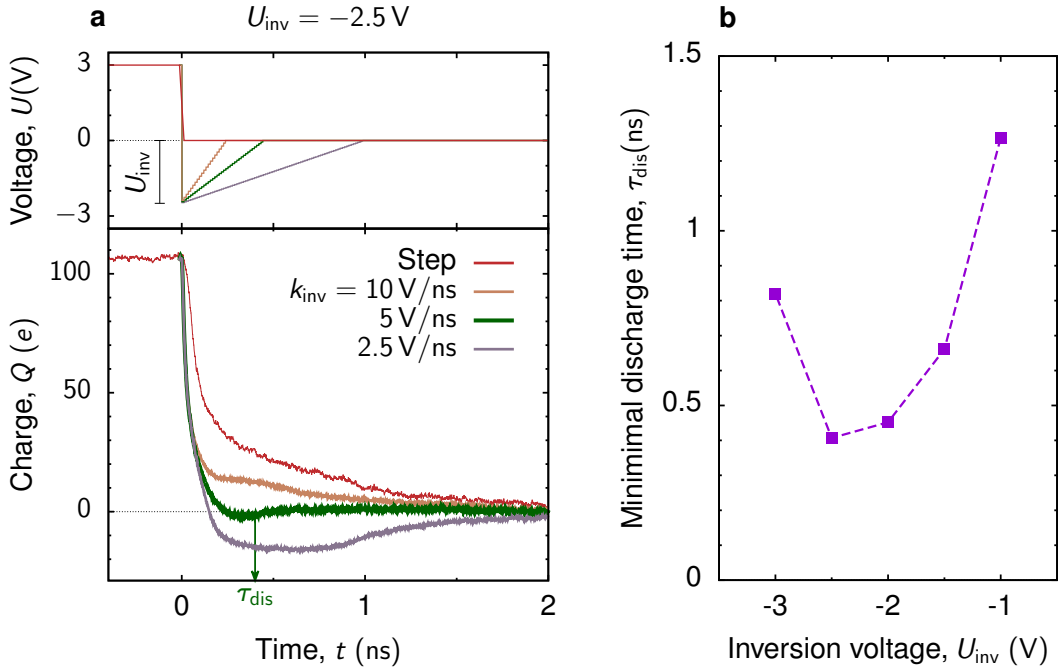

FIG. 6. **Accelerating discharging by voltage inversion**. **a**, Voltage with respect to the bulk electrolyte as a function of time for step-voltage discharging (red line) and for three voltage-inversion sweeps given by eq. (10) (top plot). Bottom plot shows the charge in the nanopore obtained by MD simulations after application of the inversion sweeps, eq. (10), to a model supercapacitor shown in Fig. 1d. The nanopore was initially fully charged at potential $U_{ch} = 3\,V$ with respect to the bulk electrolyte. The inversion voltage is $U_{inv} = -2.5\,V$, and the *optimal* k_{inv} value is $k_{inv} = 5.5\,V/ns$. The results are an average of 5 independent simulations. **b**, Discharging time as a function of U_{inv}, calculated at optimal k_{inv} values. The resulting optimal (U_{inv}, k_{inv}) pair is $(-2.5\,V, 5.5\,V/ns)$. In all plots the pore width is $w = 0.6\,nm$ and the length $\ell = 12\,nm$.

proceeds similarly as in the case of step voltage (Fig. 5g-i; step voltage not shown, but *cf.* Fig. 6a). This suggests that for each inversion voltage, U_{inv}, there must be a single optimal k_{inv} that minimizes the discharging time (for this U_{inv}).

We then optimized discharging over k_{inv} for a set of inversion voltages U_{inv}. The optimal k_{inv} was determined as k_{inv} providing the minimum discharging time, defined as the time at which the charge Q vanishes and exhibits only small fluctuations around $Q = 0$ (it is possible that the charge crosses zero and then decays to $Q = 0$ from the other side).

Simulation results for fixed U_{inv} are shown in Fig. 6a, in which we compare a few voltage-inversion discharging curves with the step-voltage discharging. Similar to the number of co and counter-ions, also the charge overshoots when the inversion voltage is applied for too long ($k_{\mathrm{inv}} = 2.5\,\mathrm{V/ns}$ in Fig. 6a, corresponding to $\tau_{\mathrm{inv}} = 1\,\mathrm{ns}$, see also Fig. 5a-c). Conversely, for high k_{inv}, discharging proceeds akin to the charge response to a step-voltage, albeit slightly faster (compare $k_{\mathrm{inv}} = 10\,\mathrm{V/ns}$ and Step in Fig. 6a). Remarkably, the optimal k_{inv} ($k_{\mathrm{inv}} \approx 5.5\,\mathrm{V/ns}$ in Fig. 6a) provides a *few-fold shorter* discharging time, as compared to the step-voltage (approximately 0.4 ns and 1.5 ns, respectively).

In Fig. 6b we plot discharging times, calculated at optimal k_{inv} values, as a function of the inversion voltage U_{inv}. This figure clearly demonstrates that there is a global minimum in the discharging times, obtained at $U_{\mathrm{inv}} \approx -2.5\,\mathrm{V}$ for our model supercapacitor. For higher U_{inv} and high k_{inv}, the inversion voltage induces overshooting that is too strong (Fig. 5e,f), while for lower U_{inv} the system 'undershoots' and discharging proceeds similarly as in the case of step-voltage (Fig. 5d,e).

We thus conclude that a voltage step does not provide the minimal discharging time, τ_{dis}, while the voltage inversions, given by eq. (10), can be optimized to yield few-fold lower τ_{dis} values.

Experimental results

With the same supercapacitor based on the novolac-derived porous carbons (Fig. 1a,b), we carried out systematic experiments to validate the MD predictions that voltage inversion can accelerate discharging. In Fig. 7 we compare a reference step-voltage discharge ($U_{\mathrm{inv}} = 0\,\mathrm{V}$) with two voltage inversions. We chose $U_{\mathrm{inv}} = -2.5\,\mathrm{V}$ based on the MD simulation results (Fig. 6), but the values of k_{inv} for the experimental setup had to be taken much larger than k_{inv} used for the single nanopore of the MD simulations. Figure 7 demonstrates that the voltage inversions discharge the supercapacitor much faster than the voltage step back.

Interestingly, we observed that, for the voltage inversions, the charge on the electrode becomes negative at intermediate times, after which it becomes positive again. We have not seen this qualitative feature so well pronounced in the MD simulations (compare with the green curve in Fig. 6). One likely has to account for ionic currents in the quasi-neutral macropores of the porous electrodes [51], which are ignored in our MD simulations.

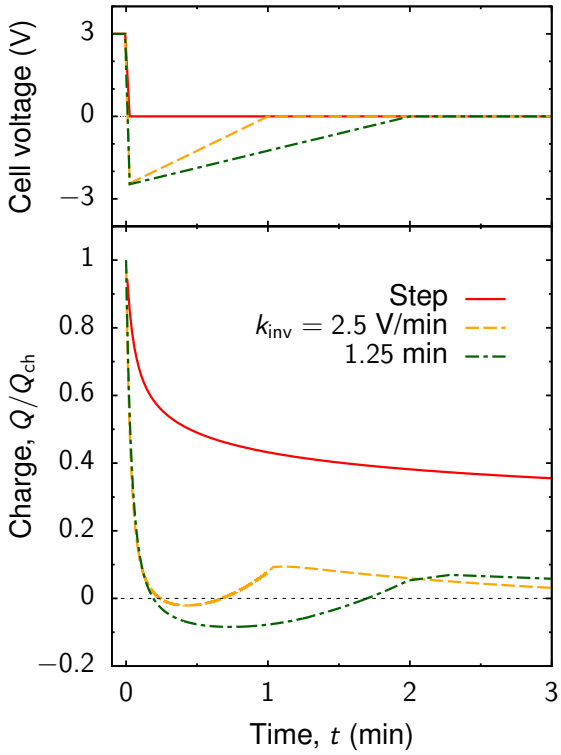

FIG. 7. **Accelerating discharging by voltage inversion for novolac-derived carbons.** Cell voltage as a function of time for step-voltage discharging (red line) and for two voltage-inversion sweeps given by eq. (10) with $U_{\rm inv} = -2.5\,\mathrm{V}$ (top plot). The bottom plot shows the accumulated charge after application of the discharging protocols from the top plot. The supercapacitor was initially charged with a step voltage for about 1 h at cell voltage $U_{\rm ch} = 3\,\mathrm{V}$.

CONCLUSIONS

It has been shown by molecular dynamics (MD) simulations that when a step-voltage is applied to an electrode with subnanometre pores, the quickly adsorbed counter-ions clog the pore entrance and lead to co-ion trapping, causing sluggish charging dynamics [47, 48]. In a recent work [42] it has been suggested that clogging can be avoided by applying the potential difference slowly via an optimized linear sweep. Here, we have demonstrated that one may achieve even *faster* charging by adjusting the rate of voltage variation to the rate of co-ion desorption. We presented a general expression for such a non-linear voltage sweep (via inversion of eq. (2)) and considered two closed-formed approximations, eqs. (6) and (9). These approximate expressions depend on three and two parameters, respectively, which in

practical applications can be treated as optimization variables. With MD simulations, we showed that the *optimized* non-linear sweep can indeed provide a significantly faster charging (Fig. 3). The gain in the charging time over the linear optimal sweep increases for increasing pore length (Fig. 3c), which suggests that the non-linear sweeps can be particularly relevant for realistically long nanopores. We showed experimentally with novolac-derived porous carbons that slow voltage sweeps indeed provide faster charging (Fig. 4), but more work needs to be done to differentiate the linear and non-linear protocols in the regime of full charging.

For discharging we have found that the uncharged state could be reached much faster than diffusively. This might seem surprising given that no electrostatic driving force acts on the in-pore ions. However, applying a 'negative' potential difference to an electrode (*i.e.*, opposite in sign to the potential of a charged state) removes counter-ions from the pore-entrance, effectively speeding up their desorption while also accelerating the adsorption of bulk co-ions into the pores (Fig. 5). We optimized the discharging time of such a two-parameter *voltage inversion* procedure, in which the applied potential steps to a negative value and recovers to zero with a linear voltage increase (eq. (10)). Using MD simulations, we observed a few-fold decrease in discharging times, as compared to the purely diffusive step-voltage discharging (Fig. 6). We verified in experiments with the novolac-derived porous electrodes that voltage inversion can indeed provide much faster discharging. The finding that discharging can be accelerated may find a useful application in capacitive deionization, where for the production of potable water via ion electrosorption, the operation speed is a very important factor.

We thank Jakob Krummacher for fruitful discussions. M.J. and S.K. acknowledge support from S. Dietrich (MPI-IS, Stuttgart). V.P. and P.S. thank Eduard Arzt (INM) for his continued support. C.H and K.B were funded by Deutsche Forschungsgemeinschaft (DFG, German Research Foundation) under Germany's Excellence Strategy - EXC 2075 - 390740016, and through Project Number 327154368 – SFB 1313.

AUTHOR CONTRIBUTION

S.K., C.H. and K.B. initiated the research. K.B. performed the simulations. V.P. designed and supervised the experimental work, P.S. performed the experiments, and B.L.M. did the

TEM analysis. S.K. and M.J. derived the equations and drafted the manuscript. All authors contributed to the discussion of the results and editing of the manuscript.

METHODS

Simulations

We have carried out MD simulations with the simulation package ESPResSo (version 3.3.1) [54–57]. The electrode geometry was built with carbon particles based on a triangular mesh of the slit-shaped surface, resulting in a hexagonal carbon structure. Throughout the study, we used the following parameters: Pore entrance radii of 4 Å, pore closing radii of 2 Å, an accessible pore width of 0.6 nm, and an electrode separation (or bulk size) of 8 nm. We used pore lengths of 12 nm, 16 nm and 20 nm for our study of the charging behaviour, whereas a single pore length of 12 nm was used in the discharging part.

We used the ICC* algorithm [58] to carry out constant-potential simulations. The ICC* method recalculates the charges on the carbon atoms every time step (2 fs) to model metallic boundary conditions and charge induction caused by ions. This was supplemented by the pre-calculated electrostatic potential ϕ (varying in space) due to the voltage applied between the two electrodes; ϕ was obtained by solving the Laplace equation [59] of the respective electrode geometry with a reference potential drop (between the electrodes) of 1 V, which was rescaled in accord with a time-dependent potential difference during a simulation.

To gain computational efficiency and consistency with previous studies [42, 48, 60–64], we used the Weeks-Chandler-Anderson (WCA) potential for the interactions between all particle species. We chose the parameters of this soft-core repulsive interaction as follows: $\sigma_c = 3.37\,\text{Å}$ and $\epsilon_c = 1\,\text{kJ/mol}$ (carbon atoms) and $\sigma = 5\,\text{Å}$ and $\epsilon = 1\,\text{kJ/mol}$ (ions), *i.e.*, the monovalent ions were treated as symmetric WCA particles.

We used the velocity-Verlet algorithm [65] in the NVT ensemble to propagate the system and a Langevin thermostat at temperature $T = 400\,\text{K}$ and damping constant $\xi = 10\,\text{ps}^{-1}$. The thermalization dissipates the temperature increase due to Ohmic losses that appear during charging [66, 67]. This also alters the dynamics of the system, so the choice of T and ξ will have an impact on the time characteristics such as the charging times presented here. Even though absolute values will depend on the NVT parameters, inter-system comparisons

using the same thermostat setup are still valuable. In all simulations of charging, the system was first equilibrated for 4 ns without applied potential before a production run.

Experiments

Synthesis of Novolac-derived carbon

The synthesis of Novolac-derived carbon involves three main steps following our previous study [50]. Briefly, we first crosslinked our polymer precursor using a solvothermal technique. 20 g of Novolac (ALNOVOL PN320, Allnex) was dissolved in 100 mL ethanol. Then, 2.5 g of crosslinker (hexamethylenetetramine) was dissolved in 500 mL mili-Q water. The novolac solution was then added to the crosslinker solution in a 1 L autoclave container. At this step, one can observe the colour of the mixed solution changed from colourless to milky solution indicating the self-emulsion process. Before heating the autoclave, the container was filled with N_2 gas to avoid oxidation of our polymer solution. Then, the autoclave was heated to 150 °C with the heating rate of 5 °C/ min. The autoclave was held at 150 °C for 8 h and passively cooled down to room temperature. The as-obtained sample was freeze-dried using liquid nitrogen to obtain novolac-beads. As for the second step, we pyrolyzed novolac-beads under an argon atmosphere at 700 °C using a heating rate of 2 °C/ min. The pyrolysis time was 2 h. To enlarge the pore of carbon, as well as to enhance the surface area of carbon, the CO_2 activation was necessary. The sample was subjected into the tubular furnace and heated to 1000 °C, while feeding CO_2 gas with the constant flow rate of 100 cm^3/ min. The activation time was 2 h. The activated Novolac-derived carbon was named PNC-2h.

Material characterization

The electron micrograph of PNC-2h was obtained via field emission scanning electron microscope (SEM; JEOL-JSM-7500F, JEO Ltd.). Nitrogen gas sorption analysis was performed with a Quantachrome Autosorb iQ system. Before nitrogen sorption, the sample was vacuum degassed at 200 °C for 1 h. After, the sample was heated to 300 °C and hold at such temperature for 20 h at the relative pressure of 0.1 Pa. Yet, the sample are volatile free. We then conduct the nitrogen sorption analysis at the temperature of −196 °C using liquid nitrogen. The relative pressure of the nitrogen was increased from 5×10^{-7} to 1.0 in

79 steps. A quenched-solid density functional theory (QSDFT) was used to calculate the pore size distribution (PSD) assuming slit-like pores.

The scanning transmission electron microscope (STEM) experiments were performed in the bight field mode on a JEOL Cs corrected ARM operated at 200 kV equipped with a cold field-emission microscope with a nominal 0.1 nm probe size under standard operating conditions.

Electrode preparation and cell assembling

We used free-standing polymer-bound electrode produced as outlined in previous work [50, 68]. To this end, the carbon material PNC-2h was dispersed in ethanol. The mixture was stirred for 5 min, then polytetrafluorethylene (PTFE; 60 mass % in H_2O) was added into the carbon-ethanol mixture. The slurry was constantly mixed in the motor until the ethanol was evaporated. The dough-like carbon paste was then pressed into the squarish shape and rolled using the rolling machine to adjust the thickness of the electrode to 120 μm (wet-thickness). The carbon electrode was then dried in the vacuum oven at 120 °C overnight. The resulting electrode consist of 90 mass % carbon and 10 mass % of PTFE. The dry thickness of our working electrode was ca. 100 μm.

We conducted the electrochemistry measurement using our custom-built cell, as described elsewhere [68]. We used full-cell symmetrical two-electrode setup having PNC-2h electrode as the working and counter electrode. First, PNC-2h electrode was cut in a disk with a diameter of 12 mm. This electrode was attached to a graphite-coated aluminium current collector of the same diameter having the thickness of 37 µm. A 13 mm in diameter glass fibre (GF/F Whatman) was used as separator. After putting all the component into the body of the cell, the cell was tightly closed using spring-loaded titanium piston while leaving hold at the side of the cell open. The cell was then dried in the vacuum oven at 120 °C overnight to remove the residual humidity. Finally, the dried cell was filled by the ionic liquid (EMIM-BF_4) in an MBraun Argon-filled glovebox (O_2, $H_2O < 1$ ppm).

REFERENCES

* M.J. present address: Mechanics Division, Department of Mathematics, University of Oslo, 0316 Oslo, Norway.

[1] J. R. Miller and P. Simon, Materials science ? electrochemical capacitors for energy management, Science **321**, 651 (2008).

[2] P. Simon and Y. Gogotsi, Materials for electrochemical capacitors, Nature materials **7**, 845 (2008).

[3] F. Béguin, V. Presser, A. Balducci, and E. Frackowiak, Carbons and electrolytes for advanced supercapacitors, Advanced Materials **26**, 2219 (2014).

[4] A. González, E. Goikolea, J. A. Barrena, and R. Mysyk, Review on supercapacitors: Technologies and materials, Renewable and Sustainable Energy Reviews **58**, 1189 (2016).

[5] D. Brogioli, Extracting renewable energy from a salinity difference using a capacitor, Physical Review Letters **103**, 10.1103/physrevlett.103.058501 (2009).

[6] A. Härtel, M. Janssen, D. Weingarth, V. Presser, and R. van Roij, Heat-to-current conversion of low-grade heat from a thermocapacitive cycle by supercapacitors, Energy Environ. Sci. **8**, 2396 (2015).

[7] C. Gao, S. W. Lee, and Y. Yang, Thermally regenerative electrochemical cycle for low-grade heat harvesting, ACS Energy Letters **2**, 2326 (2017).

[8] S. Porada, R. Zhao, A. van der Wal, V. Presser, and P. Biesheuvel, Review on the science and technology of water desalination by capacitive deionization, Progress in Materials Science **58**, 1388 (2013).

[9] M. E. Suss and V. Presser, Water desalination with energy storage electrode materials, Joule **2**, 10 (2018).

[10] Y. Zhang, P. Srimuk, M. Aslan, M. Gallei, and V. Presser, Polymer ion-exchange membranes for capacitive deionization of aqueous media with low and high salt concentration, Desalination **479**, 114331 (2020).

[11] A. Al-zubaidi, X. Ji, and J. Yu, Thermal charging of supercapacitors: a perspective, Sustainable Energy & Fuels **1**, 1457 (2017).

[12] J. Krummacher, C. Schütter, L. Hess, and A. Balducci, Non-aqueous electrolytes for electrochemical capacitors, Current Opinion in Electrochemistry **9**, 64 (2018).

[13] J. Chmiola, G. Yushin, Y. Gogotsi, C. Portet, P. Simon, and P. L. Taberna, Anomalous increase in carbon capacitance at pore sizes less than 1 nanometer, Science **313**, 1760 (2006).

[14] E. Raymundo-Piñero, K. Kierczek, J. Machnikowski, and F. Béguin, Relationship between the nanoporous texture of activated carbons and their capacitance properties in different electrolytes, Carbon **44**, 2498 (2006).

[15] C. Largeot, C. Portet, J. Chmiola, P.-L. Taberna, Y. Gogotsi, and P. Simon, Relation between the ion size and pore size for an electric double-layer capacitor, Journal of the American Chemical Society **130**, 2730 (2008).

[16] S. Kondrat, C. R. Pérez, V. Presser, Y. Gogotsi, and A. A. Kornyshev, Effect of pore size and its dispersity on the energy storage in nanoporous supercapacitors, Energy & Environmental Science **5**, 6474 (2012).

[17] G. Feng, R. Qiao, J. Huang, B. G. Sumpter, and V. Meunier, Atomistic insight on the charging energetics in subnanometer pore supercapacitors, Journal of Physical Chemistry C **114**, 18012 (2010).

[18] P. Wu, J. Huang, V. Meunier, B. G. Sumpter, and R. Qiao, Complex capacitance scaling in ionic liquids-filled nanopores, ACS Nano **5**, 9044 (2011).

[19] S. Kondrat and A. Kornyshev, Superionic state in double-layer capacitors with nanoporous electrodes, Journal of Physics: Condensed Matter **23**, 022201 (2011).

[20] P. Wu, J. Huang, V. Meunier, B. Sumpter, and R. Qiao, Voltage dependent charge storage modes and capacity in sub-nanometer pores, Journal of Physical Chemistry Letters **3**, 1732 (2012).

[21] C. Merlet, B. Rotenberg, P. A. Madden, P.-L. Taberna, P. Simon, Y. Gogotsi, and M. Salanne, On the molecular origin of supercapacitance in nanoporous carbon electrodes, Nature Materials **11**, 306 (2012).

[22] L. Xing, J. Vatamanu, O. Borodin, and D. Bedrov, On the atomistic nature of capacitance enhancement generated by ionic liquid electrolyte confined in subnanometer pores, Journal of Physical Chemistry Letters **4**, 132 (2013).

[23] H. Wang, A. C. Forse, J. M. Griffin, N. M. Trease, L. Trognko, P.-L. Taberna, P. Simon, and C. P. Grey, In situ nmr spectroscopy of supercapacitors: Insight into the charge storage mechanism, Journal of the American Chemical Society **135**, 18968 (2013).

[24] A. C. Forse, J. M. Griffin, H. Wang, N. M. Trease, V. Presser, Y. Gogotsi, P. Simone, and

C. P. Grey, Nuclear magnetic resonance study of ion adsorption on microporous carbide-derived carbon, Physical Chemistry Chemical Physics **15**, 7722 (2013).

[25] J. M. Griffin, A. C. Forse, W.-Y. Tsai, P.-L. Taberna, P. Simon, and C. P. Grey, In situ nmr and electrochemical quartz crystal microbalance techniques reveal the structure of the electrical double layer in supercapacitors, Nature Materials **14**, 812 (2015).

[26] A. A. Lee, D. Vella, A. Goriely, and S. Kondrat, Capacitance-power-hysteresis trilemma in nanoporous supercapacitors, Physical Review X **6**, 021034 (2016).

[27] A. C. Forse, C. Merlet, J. M. Griffin, and C. P. Grey, New perspectives on the charging mechanisms of supercapacitors, Journal of the American Chemical Society **138**, 5731 (2016).

[28] Z. Li, T. Mendez-Morales, and M. Salanne, Computer simulation studies of nanoporous carbon-based electrochemical capacitors, Current Opinion in Electrochemistry **9**, 81 (2018).

[29] L. Xing, J. Vatamanu, G. D. Smith, and D. Bedrov, Nanopatterning of electrode surfaces as a potential route to improve the energy density of electric double-layer capacitors: Insight from molecular simulations, Journal of Physical Chemistry Letters **3**, 1124 (2012).

[30] C. Merlet, C. Péan, B. Rotenberg, P. A. Madden, B. Daffos, P.-L. Taberna, P. Simon, and M. Salanne, Highly confined ions store charge more efficiently in supercapacitors, Nature communications **4** (2013).

[31] J. Vatamanu, Z. Hu, D. Bedrov, C. Perez, and Y. Gogotsi, Increasing energy storage in electrochemical capacitors with ionic liquid electrolytes and nanostructured carbon electrodes, Journal of Physical Chemistry Letters **4**, 2829 (2013).

[32] J. Vatamanu, M. Vatamanu, and D. Bedrov, Non-faradic energy storage by room temperature ionic liquids in nanoporous electrodes, ACS Nano **9**, 5999 (2015).

[33] S. Kondrat and A. Kornyshev, Pressing a spring: What does it take to maximize the energy storage in nanoporous supercapacitors?, Nanoscale Horizons **1**, 45 (2016).

[34] M. Salanne, B. Rotenberg, K. Naoi, K. Kaneko, P.-L. Taberna, C. P. Grey, B. Dunn, and P. Simon, Efficient storage mechanisms for building better supercapacitors, Nature Energy **1**, 16070 (2016).

[35] R. Burt, K. Breitsprecher, B. Daffos, P.-L. Taberna, P. Simon, G. Birkett, X. S. Zhao, C. Holm, and M. Salanne, Capacitance of nanoporous carbon-based supercapacitors is a trade-off between the concentration and the separability of the ions, The Journal of Physical Chemistry Letters **7**, 4015 (2016).

[36] O. A. Vasilyev, A. A. Kornyshev, and S. Kondrat, Connections matter: On the importance of pore percolation for nanoporous supercapacitors, ACS Appl. Energy Mater. 10.1021/acsaem.9b01069 (2019).

[37] S. Kondrat and A. Kornyshev, Charging dynamics and optimization of nanoporous supercapacitors, Journal of Physical Chemistry C **117**, 12399 (2013).

[38] S. Kondrat, P. Wu, R. Qiao, and A. A. Kornyshev, Accelerating charging dynamics in subnanometre pores, Nature materials **13**, 387 (2014).

[39] C. Péan, C. Merlet, B. Rotenberg, P. A. Madden, P.-L. Taberna, B. Daffos, M. Salanne, and P. Simon, On the dynamics of charging in nanoporous carbon-based supercapacitors, ACS Nano **8**, 1576 (2014).

[40] Y. He, R. Qiao, J. Vatamanu, O. Borodin, D. Bedrov, J. Huang, and B. G. Sumpter, Importance of ion packing on the dynamics of ionic liquids during micropore charging, The journal of physical chemistry letters **7**, 36 (2015).

[41] C. Péan, B. Rotenberg, P. Simon, and M. Salanne, Multi-scale modelling of supercapacitors: From molecular simulations to a transmission line model, Journal of Power Sources **326**, 680 (2016).

[42] K. Breitsprecher, C. Holm, and S. Kondrat, Charge me slowly, I am in a hurry: Optimizing charge-discharge cycles in nanoporous supercapacitors, ACS Nano **12**, 9733 (2018).

[43] V. Novotny and M. Hopper, Transient conduction of weakly dissociating species in dielectric fluids, Journal of The Electrochemical Society **126**, 925 (1979).

[44] P. Kornilovitch and Y. Jeon, Transient electrophoretic current in a nonpolar solvent, Journal of Applied Physics **109**, 064509 (2011).

[45] S. E. Feicht, A. E. Frankel, and A. S. Khair, Discharging dynamics in an electrolytic cell, Physical Review E **94**, 10.1103/PhysRevE.94.012601 (2016).

[46] M. Janssen, Curvature affects electrolyte relaxation: studies of spherical and cylindrical electrodes, arXiv.1907.06894 (2019).

[47] A. J. Pak and G. S. Hwang, Charging rate dependence of ion migration and stagnation in ionic-liquid-filled carbon nanopores, The Journal of Physical Chemistry C **120**, 24560 (2016).

[48] K. Breitsprecher, M. Abele, S. Kondrat, and C. Holm, The effect of finite pore length on ion structure and charging, The Journal of Chemical Physics **147**, 104708 (2017).

[49] A. C. Forse, J. M. Griffin, C. Merlet, P. M. Bayley, H. Wang, P. Simon, and C. P. Grey,

NMR study of ion dynamics and charge storage in ionic liquid supercapacitors, Journal of the American Chemical Society **137**, 7231 (2015).

[50] B. Krüner, J. Lee, N. Jäckel, A. Tolosa, and V. Presser, Sub-micrometer novolac-derived carbon beads for high performance supercapacitors and redox electrolyte energy storage, ACS Applied Materials & Interfaces **8**, 9104 (2016).

[51] C. Lian, M. Janssen, H. Liu, and R. van Roij, A blessing and a curse: how a supercapacitor's large capacitance causes its slow charging, PRL (accepted), arXiv preprint arXiv:1911.09924 (2019).

[52] M. Z. Bazant, K. Thornton, and A. Ajdari, Diffuse-charge dynamics in electrochemical systems, Physical Review E **70**, 021506 (2004).

[53] S. Kondrat, N. Georgi, M. V. Fedorov, and A. A. Kornyshev, A superionic state in nanoporous double-layer capacitors: insights from monte carlo simulations, Physical Chemistry Chemical Physics **13**, 11359 (2011).

[54] H. J. Limbach, A. Arnold, B. A. Mann, and C. Holm, ESPResSo – an extensible simulation package for research on soft matter systems, Computer Physics Communications **174**, 704 (2006).

[55] A. Arnold, O. Lenz, S. Kesselheim, R. Weeber, F. Fahrenberger, D. Röhm, P. Košovan, and C. Holm, ESPResSo 3.1 – molecular dynamics software for coarse-grained models, in *Meshfree Methods for Partial Differential Equations VI*, Lecture Notes in Computational Science and Engineering, Vol. 89, edited by M. Griebel and M. A. Schweitzer (Springer Berlin Heidelberg, 2013) pp. 1–23.

[56] A. Arnold, K. Breitsprecher, F. Fahrenberger, S. Kesselheim, O. Lenz, and C. Holm, Efficient algorithms for electrostatic interactions including dielectric contrasts, Entropy **15**, 4569 (2013).

[57] F. Weik, R. Weeber, K. Szuttor, K. Breitsprecher, J. de Graaf, M. Kuron, J. Landsgesell, H. Menke, D. Sean, and C. Holm, ESPResSo 4.0 – an extensible software package for simulating soft matter systems, The European Physical Journal Special Topics **227**, 1789 (2019).

[58] S. Tyagi, M. Süzen, M. Sega, M. C. Barbosa, S. S. Kantorovich, and C. Holm, An iterative, fast, linear-scaling method for computing induced charges on arbitrary dielectric boundaries, The Journal of Chemical Physics **132**, 154112 (2010).

[59] W. H. Press, *Numerical recipes: the art of scientific computing* (Cambridge Univ Pr, 2007).

[60] M. V. Fedorov and A. A. Kornyshev, Ionic liquid near a charged wall: Structure and capac-

itance of electrical double layer, The Journal of Physical Chemistry B **112**, 11868 (2008), http://pubs.acs.org/doi/pdf/10.1021/jp803440q.

[61] M. V. Fedorov and A. Kornyshev, Towards understanding the structure and capacitance of electrical double layer in ionic liquids, Electrochimica Acta **53**, 6835 (2008).

[62] K. Breitsprecher, P. Košovan, and C. Holm, Coarse-grained simulations of an ionic liquid-based capacitor I: density, ion size, and valency effects, Journal of Physics: Condensed Matter **26**, 284108 (2014).

[63] K. Breitsprecher, P. Košovan, and C. Holm, Coarse-grained simulations of an ionic liquid-based capacitor II: asymmetry in ion shape and charge localization, Journal of Physics: Condensed Matter **26**, 284114 (2014).

[64] K. Breitsprecher, K. Szuttor, and C. Holm, Electrode models for ionic liquid-based capacitors, The Journal of Chemical Physics C **119**, 22445 (2015).

[65] D. Frenkel and B. Smit, *Understanding Molecular Simulation*, 1st ed. (Academic Press, San Diego, 1996).

[66] C. Merlet, C. Péan, B. Rotenberg, P. A. Madden, P. Simon, and M. Salanne, Simulating supercapacitors: Can we model electrodes as constant charge surfaces?, The Journal of Physical Chemistry Letters **4**, 264 (2013).

[67] M. Janssen and R. van Roij, Reversible heating in electric double layer capacitors, Phys. Rev. Lett. **118**, 10.1103/physrevlett.118.096001 (2017).

[68] D. Weingarth, M. Zeiger, N. Jäckel, M. Aslan, G. Feng, and V. Presser, Graphitization as a universal tool to tailor the potential-dependent capacitance of carbon supercapacitors, Advanced Energy Materials **4**, 1400316 (2014).